Novel approach to probe ionic species mobility in molten salts electrolyte for Thermal Batteries

Clément Hachem, Luc Faget, Emmanuel Véron, Catherine Bessada, Leire del Campo, Arthur Cachot, Lionel Cosson, Vincent Sarou-Kanian, Michaël Deschamps

Journal of Power Sources 652 (2025) 237558

Contents lists available at ScienceDirect

Journal of Power Sources

journal homepage: www.elsevier.com/locate/jpowsour

Novel approach to probe ionic species mobility in molten salts electrolyte for Thermal Batteries

Clément Hachem [a,b,*], Luc Faget [a], Emmanuel Véron [b], Catherine Bessada [b], Leire Del Campo [b], Arthur Cachot [b], Lionel Cosson [b], Vincent Sarou-Kanian [b], Michaël Deschamps [b]

[a] ASB Aerospatiale Batteries, Bourges, France
[b] Université d'Orléans, CNRS, CEMHTI, (UPR3079), Orléans, France

HIGHLIGHTS

- HT-NMR coupled with EIS reveals ionic mobility in molten salt electrolytes.
- Lithium dominates conductivity in LiF-LiCl-LiBr from solid to liquid state.
- Lithium diffuses nearly twice as fast as fluorine at 500 °C in this system.
- MgO binding at 40 wt%/80 % TMD divides electrical conductivity by half.
- Pellet density critically impacts lithium mobility and conductivity.

ARTICLE INFO

Keywords:
Molten salt
Thermal batteries
Electrolyte
NMR
Self-diffusion

ABSTRACT

Molten salt electrolytes play a crucial role in thermal battery cells, offering excellent electrochemical performance and zero self-discharge at room temperature before melting. However, the transport properties of ionic species in these media are not well understood, and much remains unknown about the factors that determine the effectiveness of one electrolyte over another.

This study investigates the mobility of ionic species, particularly lithium and fluorine, in eutectic molten salt mixtures like LiF-LiCl-LiBr, commonly used in thermal batteries. Using advanced *in situ* high-temperature techniques, including high-temperature nuclear magnetic resonance (HT-NMR), pulsed field gradients (PFG), and electrochemical impedance spectroscopy (EIS), we aim to understand the ionic motion processes. The research also examines the binding of these salts with an MgO powder and the effect of compaction on retention properties.

The LiF-LiCl-LiBr eutectic shows superior ionic conductivity compared to systems like LiCl-KCl due to its higher lithium concentration and greater lithium mobility. Lithium diffuses faster than other ionic species, such as fluorine, but its high melting point of 440 °C limits its operational temperature range. The compaction rate of bound pellets is key to electrolyte performance, influencing ionic mobility. Higher compaction enhances lithium diffusion but may cause leakage above certain thresholds, depending on salt type and temperature.

This innovative approach enables rapid testing of various electrolytic compositions and binders, helping assess performance and the impact of manufacturing processes.

1. Introduction

Thermal batteries are a specific type of primary electrical generator operating at high temperatures and dedicated to highly demanding applications such as aerospace and defense. This electrochemical storage device is uncommon and differs from conventional batteries by its high specific power and storage capacity, which can exceed twenty years without performance degradation.

Their reliability, rapid activation, and resistance to extreme conditions like vibrations, mechanical or thermal shocks, and high rotation

* Corresponding author. ASB Aerospatiale Batteries, Bourges, France.
E-mail address: c.hachem@asb-group.com (C. Hachem).

https://doi.org/10.1016/j.jpowsour.2025.237558
Received 23 April 2025; Received in revised form 22 May 2025; Accepted 2 June 2025
Available online 1 July 2025

speeds make them ideal power sources for specific applications, including launchers, missiles, torpedoes, sonobuoys, drilling, aircraft emergency systems, or ejection seats [1–6].

The classic cells in these batteries consist of stacked disc-shaped electrodes, similar to those in a Volta battery. (Fig. 1). To prevent self-discharge before activation, the electrolyte disk separating the anode and cathode in electrochemical cells is composed of salts, which are solid at room temperature, inhibiting ionic transfer [7]. Heat is required to melt them, making them highly conductive and allowing the activation of the electrochemical reaction. To improve the mechanical integrity of the cells during operation, the electrolyte includes a binding agent (MgO), which significantly modifies its viscosity and conductivity [8].

Manufacturers typically use cathodes made of transition metal sulfides. For economical reasons, they often choose pyrite (FeS_2) for short-term batteries or those requiring high voltages [9]. CoS_2, which is more stable but more expensive, is preferred for long-term or high-discharge depth applications [10]. Manufacturers generally use lithium alloys, such as LiAl or $Li_{13}Si_4$ for anodes [11]. Electrodes made from lithium metal embedded in a porous matrix are preferred for applications requiring particularly high power over short periods (LAN) [12].

Thermal battery cell manufacturers select electrolytes to meet a number of requirements: a low melting point for a wide operating range, high ionic conductivity to allow intense discharges, and stability with respect to the cathodes and anodes used [7]. They generally use mixtures of alkali halides in eutectic proportions, preferably lithiated, to fulfill this role.

Two salt mixtures have thus proved their worth as electrolytes for several decades. The mixture historically used since the 1950s is the LiCl-KCl binary in eutectic proportion (≈45/55 wt%), showing a melting point close to 350 °C. Researchers have deeply characterized its electrochemical properties for numerous applications, from primary and secondary batteries [13–15] to nuclear fuel recycling [16–18]. However, the LiCl-KCl mixture encounters problems with salt solidification during intense discharges. Chemical deviation from the eutectic composition can causes KCl precipitation when the system operates at temperatures close to its melting point [7,19–22]. Another drawback of this binary mixture is its tendency to form parasitic phases, such as the "J phase" ($LiK_6Fe_{24}S_{26}Cl$), when molten salts interact with FeS_2 cathode material at elevated temperatures.

The second commonly used mixture is the ternary eutectic LiF-LiCl-LiBr, known as "all-lithium". It does not exhibit the precipitation problems or parasitic interactions observed with its LiCl-KCl analog. Although it has a higher melting point, at around 445 °C [7], its conductivity is close to twice that of the binary mixture, from the melting point and over the entire battery operating range, from 450 to 600 °C [19]. For all these reasons, this electrolytic system is best suited to applications involving intense discharges.

Thermal batteries may experience strong acceleration during operation. To prevent electrolyte leakage and short-circuiting, manufacturers add a binding agent, typically magnesia powder (MgO), to the electrolyte mixture [7,23,24]. This component helps immobilizing molten salts and form a pellet that retains its geometrical behavior throughout battery operation. Once formed, this pellet is called a separator.

The binding agent's ability to retain liquid salts and the separator's capacity to deform are crucial to maintain stable performance throughout the battery's lifetime, avoiding deleterious mechanisms and preventing cell delamination. For example, in case of insufficient binding, electrolyte leakage may occur due to the ejection of molten salts on the sides of the pellet. This can lead to voltage or current variations, the formation of high-resistance zones due to agglomeration of binding agent particles, or even, internal short-circuiting due to electrode contact or external by contact between two stacks. In the case of over-binding, the separator will exhibit reduced conductivity and poor electrode wettability, resulting in high contact resistances at the interfaces [8,25]. The amount of binding agent added to the salts generally varies from 30 to 50 wt%, depending on the salts used, their viscosity and the battery's final application. For example, an application requiring high rotational speeds requires pellets with increased binding power.

Capillary forces, generated by the framework of the oxide matrix, retain molten salts in the pellet under various thermal and mechanical stresses. [26]. These capillary forces are highly dependent on the nature

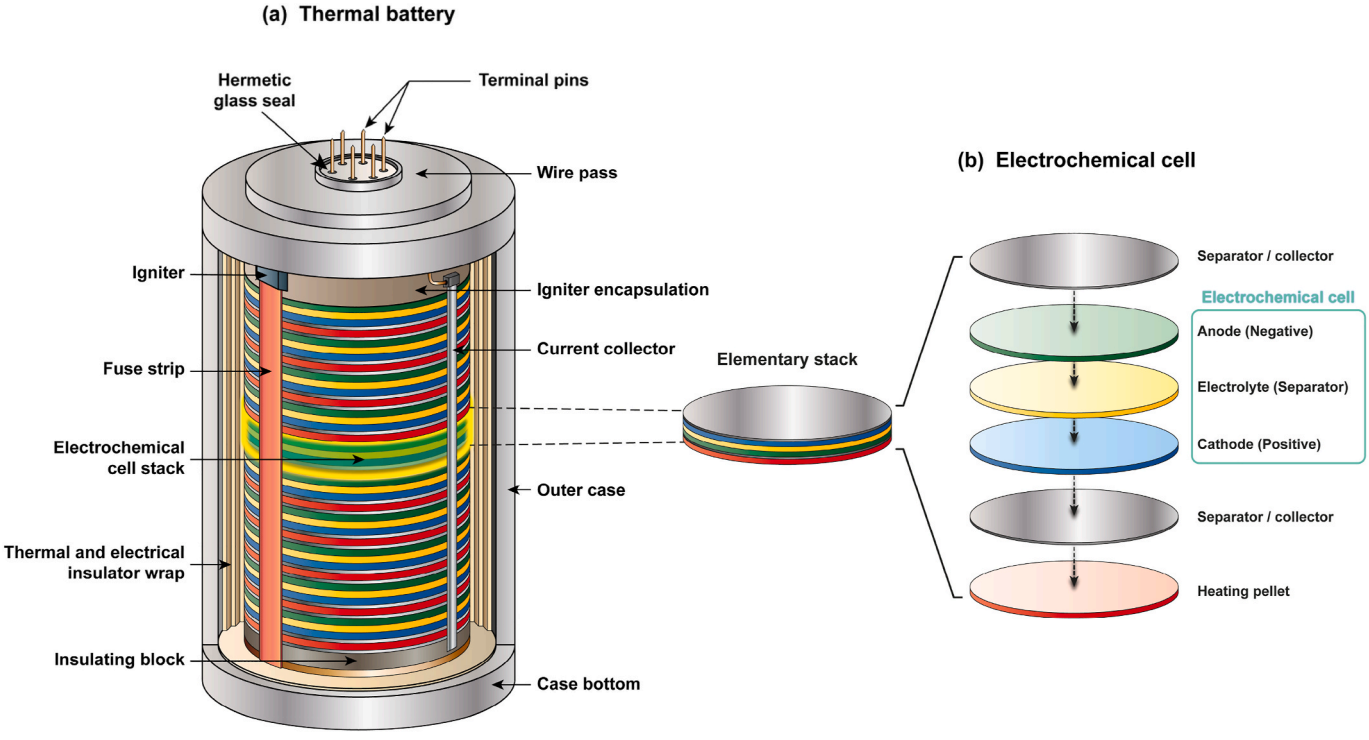

Fig. 1. (a) Global scheme of the structure of a model thermal cell with internal view. (b) Focus on the structure of the electrochemical cell.

of the binding agent and the method used to prepare the bound electrolyte. Thus, chemical composition, wettability, particle size, grain geometry, specific surface area and pore and grain size distribution are the key parameters influencing the retention properties [27]. Thus, separator pellets function as heterogeneous, unsaturated porous media consisting of ionically conductive liquid phases, a resistive insulating matrix, and pores that may form a connected network and may or may not contain salts [28].

Numerous studies are currently focusing on improving thermal batteries separators to optimize their performance. There are several possible approaches to optimization. The first is to develop new salts with higher ionic conductivities or lower melting temperatures, thereby extending the operating range and lifetime of the battery [29–31]. The second focuses on improving the binder, either by functionalizing it [32–34], or by other phases than MgO offering better salt retention capacities (Al_2O_3, ZrO_2, Y_2O_3, BN) [35–38]. The aim is to reduce the proportion of binding agent to improve separator conductivity while maintaining mechanical strength.

This work is part of this approach to optimize separator performance and collect useful data for molecular dynamics simulation. The overall aim is to develop a methodology for evaluating and comparing the performance of different electrolytes and binding agents. In addition, we aim to study the impact of various parameters, such as the chemical reactivity, the amount of binder and the degree of pellet compaction, on separator performance. Nuclear magnetic resonance (NMR), coupled with *in situ* heating of the sample, is a powerful characterization technique that has demonstrated its ability to probe the structure of salts, from the solid to the liquid state, and to measure the mobility of ionic species as a function of temperature [39–41].

Our new methodological approach to study thermal battery electrolytes couples advanced *in situ* characterization techniques. These include high-temperature NMR [42], and 4-electrode impedance spectroscopy [43], which provide detailed information on these systems. To demonstrate the feasibility of our approach, we applied it to the LiF-LiCl-LiBr eutectic. The study focuses on the mobility of ionic species and the impact of adding MgO binding agent on it.

2. Experimental

2.1. Materials

2.1.1. Salts

ASB Aerospatiale Batteries prepared and supplied the salt mixtures directly in eutectic proportions. They also provided high-purity precursors separately as reference and calibration materials for high-temperature NMR.

Given the highly hygroscopic nature of the bromide and chloride salts, after preparation they were dried overnight in a vacuum oven at 150 °C, then packaged in sealed pouches under argon before being transferred to a Jacomex glovebox under argon for storage and preparation (O_2 and H_2O below 1 ppm). Table 1 summarizes the compositions and some physicochemical data of the mixes studied.

2.1.2. Bound electrolyte

ASB Aerospatiale Batteries also prepared and supplied the bound electrolyte mixtures and the binding agent alone. The salts mix with the binding agent above their melting point to homogenize the composition. After cooling, the block is ground into powder. The LiF-LiCl-LiBr ternary mixture contains approximately 40 wt% MgO as a binder. The binding agent is nanometric magnesia powder (MgO) manufactured by calcination of magnesium carbonates. On a microscopic scale, the powder tends to form micrometer-sized agglomerates. Small carbonated impurities may remain in the material due to its natural origin (<0.4 wt%). After preparation, we dried all these materials before transferring them to the glovebox.

Table 1
Composition, melting point and ionic conductivity of the salt mixtures studied.

LiF-LiCl-LiBr « All-Lithium » Ternary Mix			
Mass composition (wt %)	Molar composition (mol%)	m.p. (°C)	Ionic conductivity at 500 °C (S cm^{-1})
9.6 wt% LiF – 22 wt% LiCl – 68.4 wt% LiBr	22 mol% LiF – 31 mol % LiCl – 47 mol% LiBr	444 °C [15]	3.39 [7]

2.2. Characterization techniques

2.2.1. X-ray Diffractometry (XRD)

X-ray diffraction patterns were collected using a Bruker D8 A25 diffractometer in Bragg-Brentano θ-θ configuration ($Cu_{K\alpha 1,2}$ radiation) and equipped with a 1-dimensionnal linear LynxEye XE detector. Powder samples were prepared in an argon glovebox using an airtight PMMA dome sample holder to avoid any reaction with the atmosphere.

2.2.2. Scanning electron microscopy (SEM) and energy Dispersive spectroscopy (EDS)

A fragment of a solidified eutectic ternary salt block was characterized by SEM-EDS following a melting process. Approximately 50 g of eutectic mixture—prepared by mixing powders of the three individual phases, LiF, LiCl, and LiBr—was placed into a BN crucible (Ø36 mm, 60 mm high). The crucible was then heated at 600 °C for 6 h in a sealed tubular furnace under a continuous argon flow. After cooling, the resulting solid was transferred into a glovebox and broken into coarse pieces. One of the central fragments, approximately 1 cm in size, was selected for SEM analysis.

Due to the sample's sensitivity, a Kammrath & Weiss vacuum transfer module was used to move the specimen from the glovebox to the SEM chamber without contamination. No metallization was applied. A representative area of the sample was examined. The analysis was conducted using a ZEISS Merlin Compact SEM, a field-emission gun (FEG) instrument equipped with a GEMINI I column and a QUANTAX XFlash6 EDS detector from Bruker. Operating conditions included an accelerating voltage of 15 kV and a working distance of 10 mm.

2.2.3. Electrochemical impedance spectroscopy (EIS)

Electrical conductivities of LiF-LiCl-KCl salt mixtures, as well as their bound versions, were measured by impedance spectroscopy using two setups: one for liquid-phase measurements, referred to as the high-temperature setup, and another for solid samples, called low-temperature setup. Both methods use a 4-electrode setup. It has the advantage of minimizing polarization effects at low frequencies and high temperatures, while limiting the contribution of wires to the measured impedance, unlike the conventional two-electrode method [41,43].

The high-temperature setup consists of a measuring probe made up of two platinum wires framed by two platinum plates, that are immersed in the liquid to be measured, which is contained in a crucible. The flow of current is imposed between the plates, while the voltage measurement takes place at the inner Pt tips. This system is contained in an alumina sheath which is introduced in a closed vertical tubular furnace that heats up to 1600 °C under air or stream of gas [44–46]. Platinum electrodes are immersed of 8 mm in the sample once it has become liquid, using a mobile micrometric system. The first measurement is taken during cooling, and the second during heating, enabling the two measurements to be compared. The temperature is measured using an S-type thermocouple located close to the sample surface.

In our case, the experiments were carried out using non-porous BN crucibles, from room temperature up to 800 °C, following a ramp of 2 °C·min^{-1}, and under argon flow. Measurement are performed with a Solartron SI 1260 impedancemeter in a frequency range from 1 Hz to 1 MHz with an applied sinusoidal voltage of 0.5 V in amplitude. The

geometrical cell factor (f_{geo}) is determined at room temperature using a 1M KCl solution of known conductivity [41,46]. Details of the experimental setup for the liquid state measurements are shown in Fig. 2 (a).

The low-temperature setup, which is designed to study solid samples, and shown in Fig. 2 (b), is based on the same experimental principle, but differs in the arrangement of the measuring probe. The setup involves pressing a sample of around 1 mm thick between two planar platinum electrodes.

The pellet is metallized on both sides using sputtered platinum before the experiment to improve electrical contact between the sample and the platinum foils. A mask controls the area covered by the sputtered metallization. By knowing the thickness of the sample (e) and the metallized surface (S) through which the current will pass, it is possible to calculate the geometrical cell factor f_{geo}, as in Eq. (1).

$$f_{geo}(\mathrm{cm}^1) = \frac{e}{S} \quad \text{Eq. 1}$$

e: Sample thickness (cm);
S: Metallized surface (cm^2).

A micrometer screw adjusts the force applied to the sample, while the measuring probe, inserted in a refractory alumina sheath, is placed in a closed vertical tubular furnace. Temperature is measured by an S-type thermocouple, located at the top of the sample.

The experiment takes place under argon flow, and the same acquisitions parameters as for the high-temperature setup are used, i.e. a frequency range from 1 Hz to 1 MHz and an applied sinusoidal voltage of 0.5 V amplitude, but this time using an AMETEK ModuLab XM MTS impedance analyzer. However, the temperature limit for experimentation with this assembly is 600 °C. Above this temperature, the platinum surface metallization degrades, resulting in a sharp rise in resistance.

Using frequency-dependent impedance data and a Nyquist plot (imaginary part vs. real part), the sample resistivity can be extracted at the intersection of the half-circle with the real axis of the resistivity. The electrical conductivity of the sample is then determined by taking the reciprocal of this value. An example of a Nyquist plot and the corresponding equivalent circuit model are provided in the Supplementary Information.

An Arrhenius plot of electrical conductivity as a function of temperature can be used to determine the activation energy of conductivity, provided the data permits. This plot type represents the logarithm of the studied value as a function of the inverse temperature. If the data follows a linear trend, the activation energy of the phenomenon can be determined from the slope of the regression using the Arrhenius' law, as described in Eq. (2):

$$\ln k = \frac{-E_a}{k_B}\left(\frac{1}{T}\right) + \ln A \quad \text{Eq. 2}$$

T: Absolute temperature (K);
A: Pre-exponential factor (s^{-1});
k: Rate constant (s^{-1});
E_a: Activation energy (eV);
k_B: Boltzmann constant → $8.617 \bullet 10^{-5}$ eV K^{-1}.

Once the Arrhenius parameters (Ea and A) have been graphically extracted from the experimental data, the electrical conductivity can be expressed using the equation presented in Eq. (3):

$$\sigma_{total} = \sigma_0 \times e^{-\left(\frac{E_a}{kT}\right)} \quad \text{Eq. 3}$$

σ_{total}: total electrical conductivity including ionic and electronic contributions ($S \cdot cm^{-1}$);
σ_0: pre-exponential conductivity factor ($S \cdot cm^{-1}$).

2.2.4. Nuclear magnetic resonance (NMR)

High-temperature NMR spectra were recorded in static mode on a Bruker Avance I 400 MHz spectrometer, generating a magnetic field of 9.4 T. *In situ* analyses were carried out using the laser heating system historically developed at CNRS-CEMHTI in Orléans, France [39,47–49]. Fig. 3 (a, b, c) illustrates the system's overall operation.

The heating system consists of two coupled CO_2 lasers, each with a power of 250 W, emitting in the infrared range (λ = 10.6 μm). These lasers heat the crucible, which contains the sample, from both sides, using ZnSe mirrors to guide the beam into the spectrometer and the probe.

This avoids temperature gradients in the sample. Laser power is

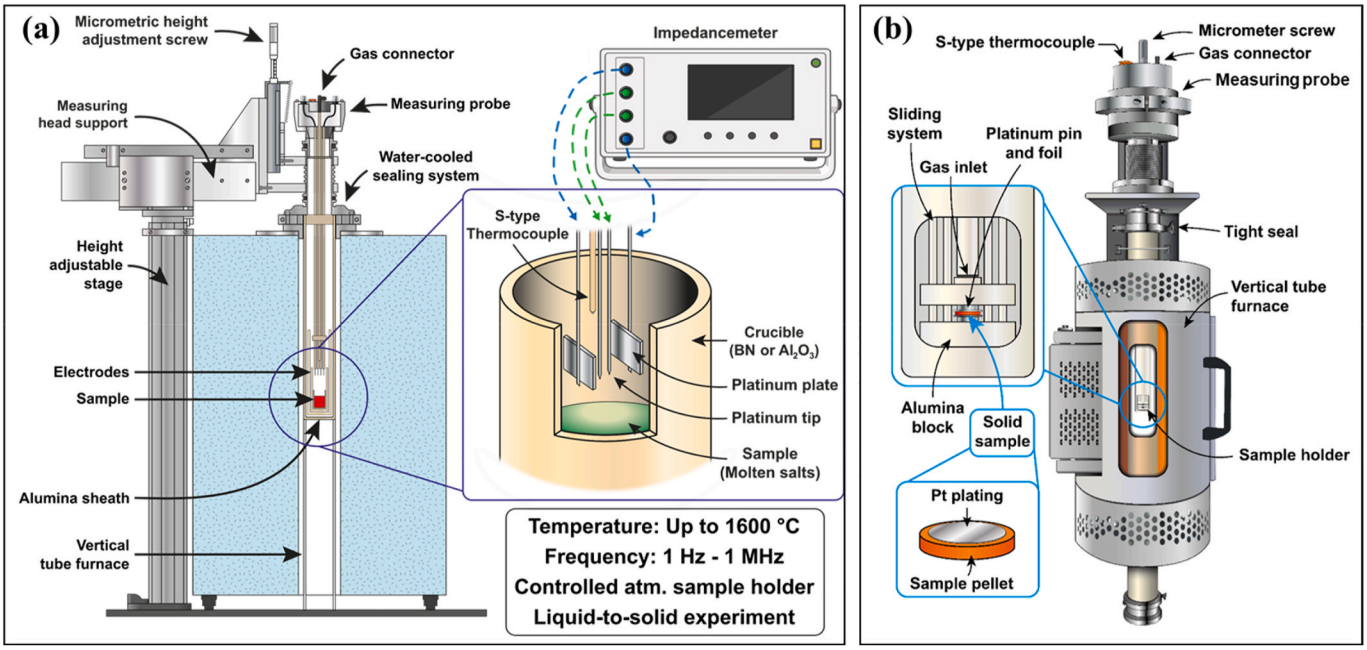

Fig. 2. (a) Four-electrode EIS system for high-temperature analysis of liquid samples. (b) EIS setup for solid samples analysis at high temperature.

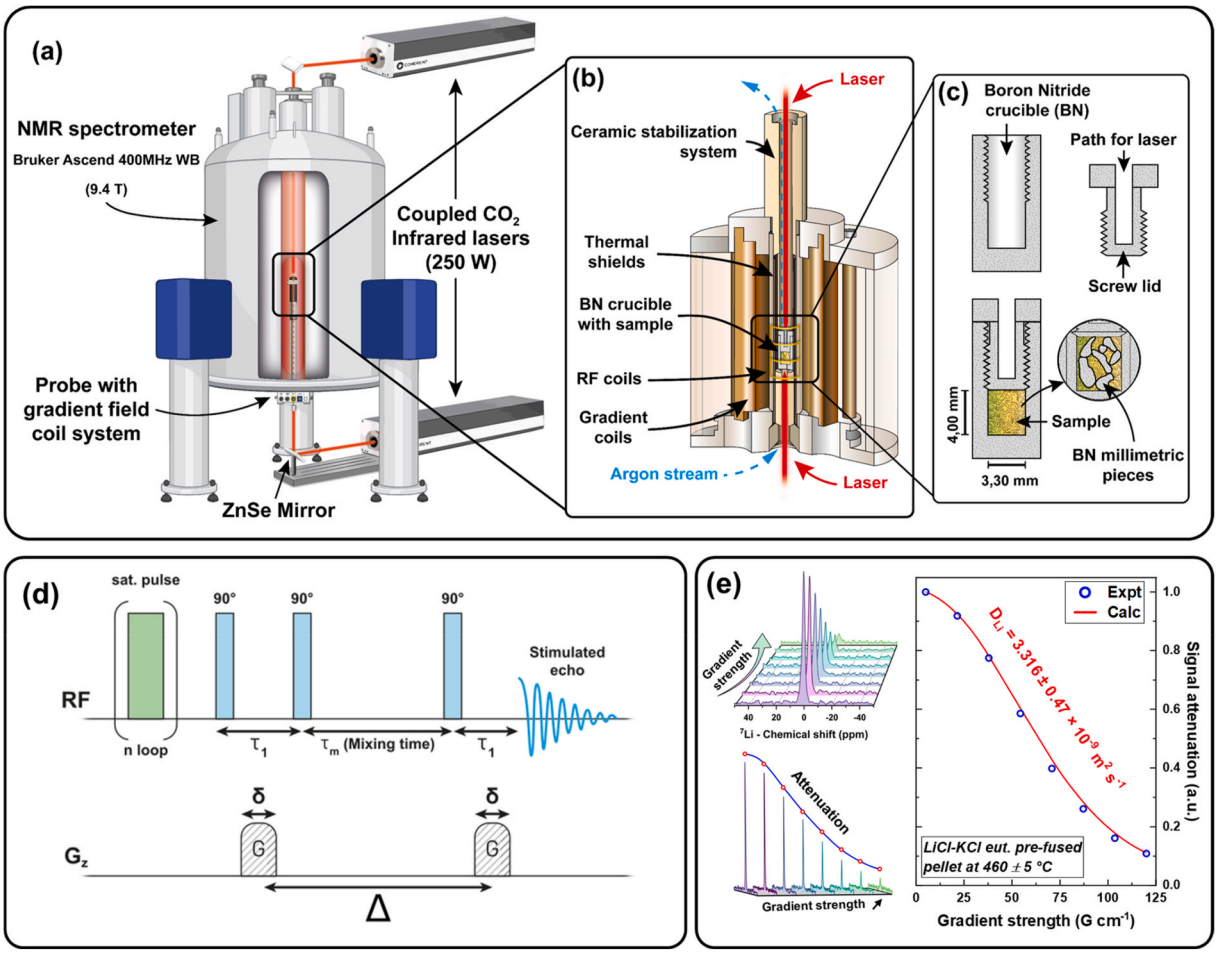

Fig. 3. (a) High-Temperature NMR *in situ* laser heating setup with diffusion probe. (b) Focus on the sample area. (c) NMR specially designed BN crucible. (d) PFG-STE NMR pulse sequence. (e) NMR spectra and attenuation curve.

computer-controlled, and temperature is pre-calibrated using compounds with phase transitions at specific temperatures, with an accuracy of ±5 °C. Experiments are carried out under an argon flow of approx. 2 L min^{-1} and the electronics are cooled by a strong air flow. After the experiment, the samples were weighted and analyzed by XRD to check there is no contamination. Weight loss measurements confirmed that no evaporation occurred during the experiment in closed crucible.

The study used three different NMR probes, originally designed by Bruker for liquid state analysis, which were specially modified to withstand high temperatures. Two probes were dedicated to the measurement of NMR spectra at high temperatures. They use large crucibles with a diameter of 9 mm, allowing analysis of larger sample quantities, approximately 150 mg. One probe was used for the measurement of ^{19}F, ^{7}Li and ^{81}Br nuclei, while the other was specifically dedicated to recording low-gamma nuclei spectra like ^{35}Cl.

The third probe is a modified Bruker 10 mm Diff30 probe equipped with a water-cooled gradient coil which can generate a magnetic field gradient up to 1200 G cm^{-1}. The crucibles used with this probe are smaller, about 6 mm in diameter, and can hold about 50–70 mg of sample.

For each system studied, spectra were acquired for the nuclei present in the sample at different temperatures using a conventional single pulse sequence. An equilibration time of 5 min was observed after each temperature change, before starting a new pulse sequence.

Self-diffusion coefficient measurements were carried out only on ^{7}Li and ^{19}F, as other nuclei have too low Larmor frequencies or too short relaxation time, and only when the samples are in liquid state. The pulsed field gradient (PFG) method, a stimulated echo sequence, preceded by a saturation train, and coupled to gradient pulses, is used for this purpose [50].

It is schematically illustrated in Fig. 3 (d). The sequence is repeated eight times with a gradual increase in gradient strength to obtain a single value for the self-diffusion coefficient at a given temperature. The value is determined by fitting of the signal attenuation curve, as in Fig. 3 (e), according to the Stejskal-Tanner equation (Eq. (4)) [51].

As for electrical conductivity, the temperature dependence of the self-diffusion coefficient could be expressed using Arrhenius' law, leading to Eq. (5).

$$I_g = I_0 \times e^{-D(\gamma\delta g)^2\left(\Delta-\frac{\delta}{3}\right)} \quad \text{Eq. 4}$$

γ: Gyromagnetic ratio of the targeted nucleus (Hz·G^{-1})
δ: Gradient pulse duration (s)
g: Gradient intensity (G·m^{-1})
Δ: Time between two gradient pulses (s)
I_g: Echo intensity for a g gradient intensity;
I_0: Echo intensity without application of field gradient;
D: Self-diffusion coefficient of target nucleus (m^2·s^{-1})

$$D_{ion} = D_0 \times e^{-\left(\frac{E_a}{kT}\right)} \quad \text{Eq. 5}$$

D_{ion}: self-diffusion coefficient of an ionic species (m^2·s^{-1});
D_0: pre-exponential diffusion factor (m^2·s^{-1}).

Magnetic properties, such as T_1 longitudinal relaxation time and T_2 transverse relaxation time, vary considerably from one nucleus to another. Experimental parameters are therefore adjusted individually for each nucleus, using reference compounds. The standard values are summarized in Table 2.

To minimize convection phenomena that could alter species mobility in liquid, millimetric fragments of dense BN were added in the crucible with the sample [39].

3. Results

3.1. Solid solution in the LiCl-LiBr system

The first observation in this study focuses on the diffraction patterns of samples from the LiF-LiCl-LiBr system before and after melting (Fig. 4 (a)). Initially, the system exhibits three distinct crystalline phases: LiF, LiCl and LiBr. After a first melting and cooling step, only two phases remain: LiF and one phase unidentified in the COD and PDF5+ databases. There is a disappearance of peaks associated with the pure phases of LiCl and LiBr on the diffractogram, along with the appearance of new ones. The new reflections observed after melting can be indexed in the same space group as LiCl and LiBr, but with an intermediate unit cell (determined by the LeBail method), suggesting the presence of a solid solution.

It appears that a homogeneous and continuous solid solution is formed between LiBr and LiCl when they coexist in ternary eutectic proportions, with complete substitution of the two anions, phenomenon commonly observed in other alkali halides [52].

SEM-EDS chemical analysis, presented in Fig. 4(c) and (d), show that this new solid solution is free of fluorine. The *a* lattice parameter of this new phase evolves linearly with Br content, in accordance with Vegard's law (Fig. 4 (b)). This allows us to determine the composition of the phase, which can be described by the chemical formula $Li(Br_{0.66},Cl_{0.34})$. This is close to the ratio between the base phases, with 31 mol% LiCl and 47 mol% LiBr, indicating that both salts are entirely in solid solution.

3.2. Qualitative ionic species mobility probing by HT-NMR

The narrowing of the NMR signal as a function of temperature observed in solids can be directly correlated to an increase in the mobility of the species studied [53]. This increase in motion leads to averaging of the local fields which affects the spins. A sudden variation in line width and intensity suggests a change in the mobility mechanism. The aim of this qualitative study is to highlight these variations by analyzing the NMR spectra obtained at different temperatures. The study of the LiF-LiCl-LiBr ternary eutectic by HT-NMR, from the solid to the liquid state, provides useful information on the order in which ions begin to gain mobility when temperature increases. Analyses are carried out on a perfused mixture of salts.

As shown in Fig. 5 (a), the NMR line associated with lithium in halides is very large at room temperature and doesn't really show any change until 150 °C. The first change occurs between this point and 250 °C, where the narrowing of the line indicates a first notable increase in lithium ion mobility. Thereafter, there is a plateau but the line continues to gain in intensity and become progressively sharper between 250 and 450 °C, until the eutectic mixture melts. Then, there is a second clear transition in line width during salt melting associated with a significant increase in mobility. Once the whole system is in the liquid state, the line continues to narrow slightly as the temperature rises, but the variations are less marked, indicating a continuous increase in lithium mobility, albeit in smaller proportions than those observed in the solid phase.

A study of the behavior of ^{19}F, nucleus which is present in LiF in the solid state, reveals a mobility pattern distinct from that of lithium. NMR spectra and evolution of the associated line width are shown in Fig. 5 (b). Between room temperature and 100 °C, a slight sharpening of the resonance corresponding to ^{19}F environment in LiF, located around −175 ppm, suggests a first small increase in fluorine mobility in the crystal structure.

Thereafter, the line width stabilizes and changes only slightly up to 400 °C. Above this temperature, the line sharpens significantly and increases in intensity, indicating a significant increase in mobility of ^{19}F in the solid phase. Maximum narrowing of the LiF resonance occurs during melting, between 420 and 470 °C. Thereafter, the line continues to sharpen, albeit more moderately, reflecting the continuous increase in fluorine mobility in the liquid system.

The temperature-dependent behavior of ^{35}Cl, shown in Fig. 6 (a), reveals a different trend. No resonance are detected under static conditions up to 350 °C. This is explained by the quadrupolar nature of the ^{35}Cl nucleus, which produces an extremely broad signal, making it impossible to detect when it is not very mobile. However, from 350 °C onwards, a fine, intense line appears at −4 ppm, reflecting a significant activation of chlorine mobility in the solid phase.

This activation of chlorine mobility correlates with the appearance of a line on the ^{81}Br spectrum at the same temperature. Both elements are present in the solid solution Li(Br, Cl), which explains their combined mobility. Chlorine then shows a sharpening of its line up to 630 °C, reflecting an increase in its mobility, followed by a gradual broadening from this temperature up to 850 °C.

This behavior is complex to interpret, as it suggests a decrease in chlorine mobility, which is counter-intuitive in the context of an increase in temperature. This suggests the intervention of an underlying mechanism influencing its mobility. Furthermore, a study of the longitudinal relaxation time T_1 reveals a decrease in the activation energy of relaxation, correlating with this broadening.

This type of evolution is generally interpreted as an indicator of an increase in the mobility of the species studied. This behavior could thus reflect a reaction involving the molten chlorides, for example with the boron nitride crucible, leading to the formation of complex ionic species such as $[LiCl_2]^-$ and $[Li_4N]^+$. However, no evidence of reaction could be found on ^7Li NMR spectra and X-Ray diffractograms of samples analyzed after experimentation.

^{81}Br exhibits a more predictable behavior, similar to that of fluorine, with the appearance of a line at 350 °C, indicating an activation of its mobility. This phase is followed by a progressive sharpening of the line up to 850 °C, reflecting a continuous increase in the mobility of this ionic species (Fig. 6 (b)).

3.3. Comparison with EIS conductivity measurements

The characterization of an electrolyte's electrical conductivity by impedance spectroscopy is a powerful method for assessing its performance. However, it only provides global information about the mobility of ionic species, without detailing the underlying mechanisms. This highlights a genuine interest in complementary approaches such as HT-NMR. Fig. 7 (a) shows the electrical conductivity plots obtained for the eutectic mixture of LiF-LiCl-LiBr salts as function of temperature,

Table 2
Standard acquisition conditions for high-temperature NMR experiments.

Nucleus	Larmor frequency at 9.4 T (MHz)	Pulse length (μs)	Recycle delay (s)	Number of scans	Reference
^7Li	155.506	32.5	35	16	1M LiCl in H_2O (0 ppm)
^{19}F	376.498	32	5	64	C_8H_7FO (-106.3 ppm)
^{35}Cl	39.204	52	0.5	256	1M NaCl in H_2O (0 ppm)
^{81}Br	108.061	45	0.5	256	1M NaBr in H_2O (0 ppm)

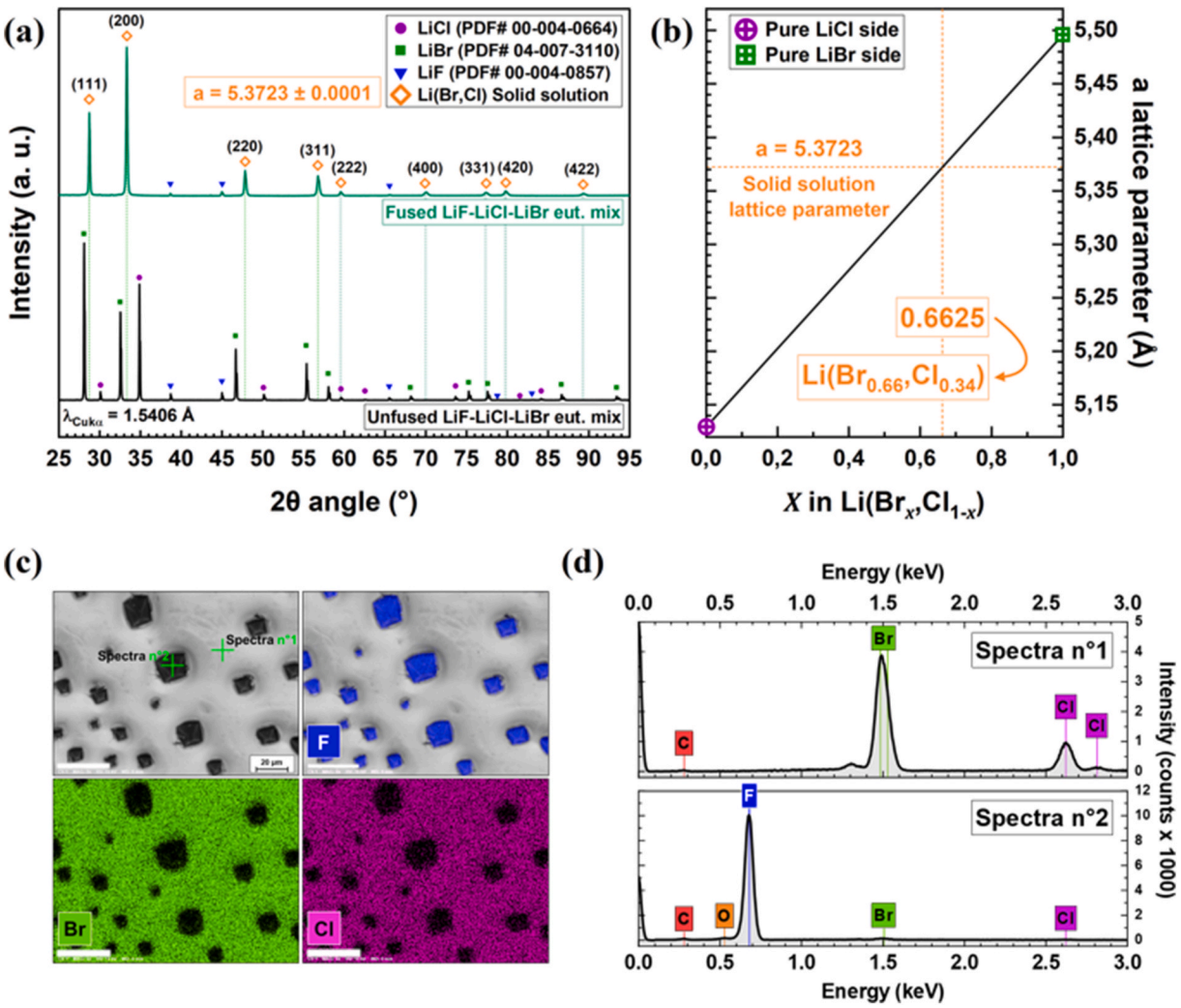

Fig. 4. (a) Comparison of powder diffraction patterns of fused and unfused LiF-LiCl-LiBr eutectic mixtures. (b) Lattice parameter vs. substituent concentration in LiCl-LiBr solid solution system. (c) SEM backscattered electron image and elemental mapping of the LiF–LiCl–LiBr eutectic pellet after melting, recorded at room temperature. (d) Corresponding EDS spectrum.

accompanied by the corresponding Arrhenius plot in Fig. 7 (b). The conductivity in these electrolyte systems is predominantly ionic in nature, with an electronic contribution considered negligible.

The graph shown in Fig. 7 (a) illustrates the evolution of conductivity in salts in their liquid state, highlighting the significant jump that occurs upon melting. However, it provides little information about the variation of electrical conductivity in the solid state, as the values in this phase range from 10^{-9} to 10^{-3} S cm^{-1}. A logarithmic scale would be more suitable for visualizing this range, but this is not the purpose of the graph, which focuses on the liquid phase corresponding to the practical operating conditions of thermal battery electrolytes.

A continuous increase in electrical conductivity is observed with rising temperature. This trend correlates with the results obtained by PFG-NMR on lithium, showing that the increase in ionic conductivity is directly linked to the enhanced mobility of lithium ions. PFG analyses also indicate that lithium is more mobile than fluorine in the melt. Furthermore, the activation energy associated with the lithium self-diffusion coefficient is comparable to the one derived from the conductivity measurements in the liquid phase, indicating that lithium is the main charge carrier in this system.

The Arrhenius plot of conductivity in Fig. 7 (b), which uses a logarithmic scale, provides a clearer representation of the variations in electrical conductivity at the solid-state. This graph identifies three distinct domains outside the liquid state, each characterized by specific activation energies.

The first domain, referred to as the “Cold Solid” region, extends from room temperature up to 180–200 °C. It corresponds to a very low conductivity range, from 10^{-9} to 10^{-6} S cm^{-1}, where the system can be considered electrically insulating.

Around 200 °C, an inflection in the slope is observed, indicating an increase in the conductivity activation energy from 0.63 eV to 1.13 eV. This significant change correlates with the onset of lithium mobility in the solid salts, as observed by HT-NMR. This second domain, dominated by lithium’s contribution to conductivity, extends from 200 °C to 350 °C, reaching conductivities on the order of 10^{-3} S cm^{-1} at its upper limit.

The third region, just before melting, is considered a transition regime. No regression is performed in this range, as the activation energy values obtained would lack clear physical meaning, since they correspond to melting and recrystallization processes. However, the abrupt change in conductivity values before and after this event reflects a significant destabilization of the system and a sharp increase in ionic mobility following melting. This regime is associated with the activation of halogen mobility, specifically chlorine and bromine, within the crystalline structure of the salts, as observed by HT-NMR. Melting occurs after fluorine begins to exhibit mobility, i.e., from 420 °C onward.

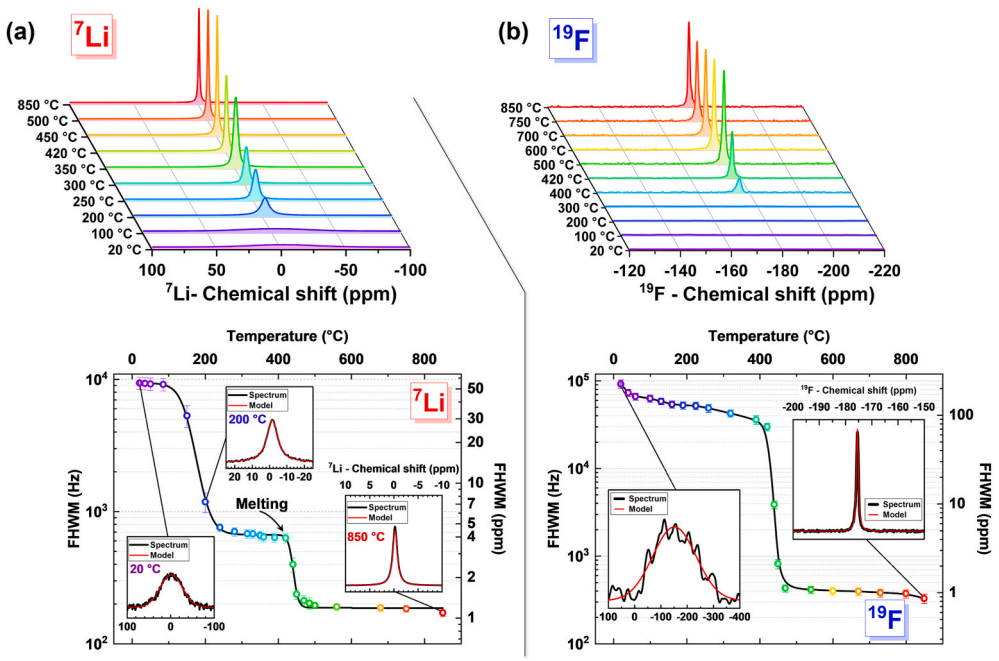

Fig. 5. (a) ^{7}Li spectra and linewidth evolution as a function of temperature. (b) ^{19}F spectra and linewidth evolution as a function of temperature (B_0 = 9.4 T, static HT-NMR).

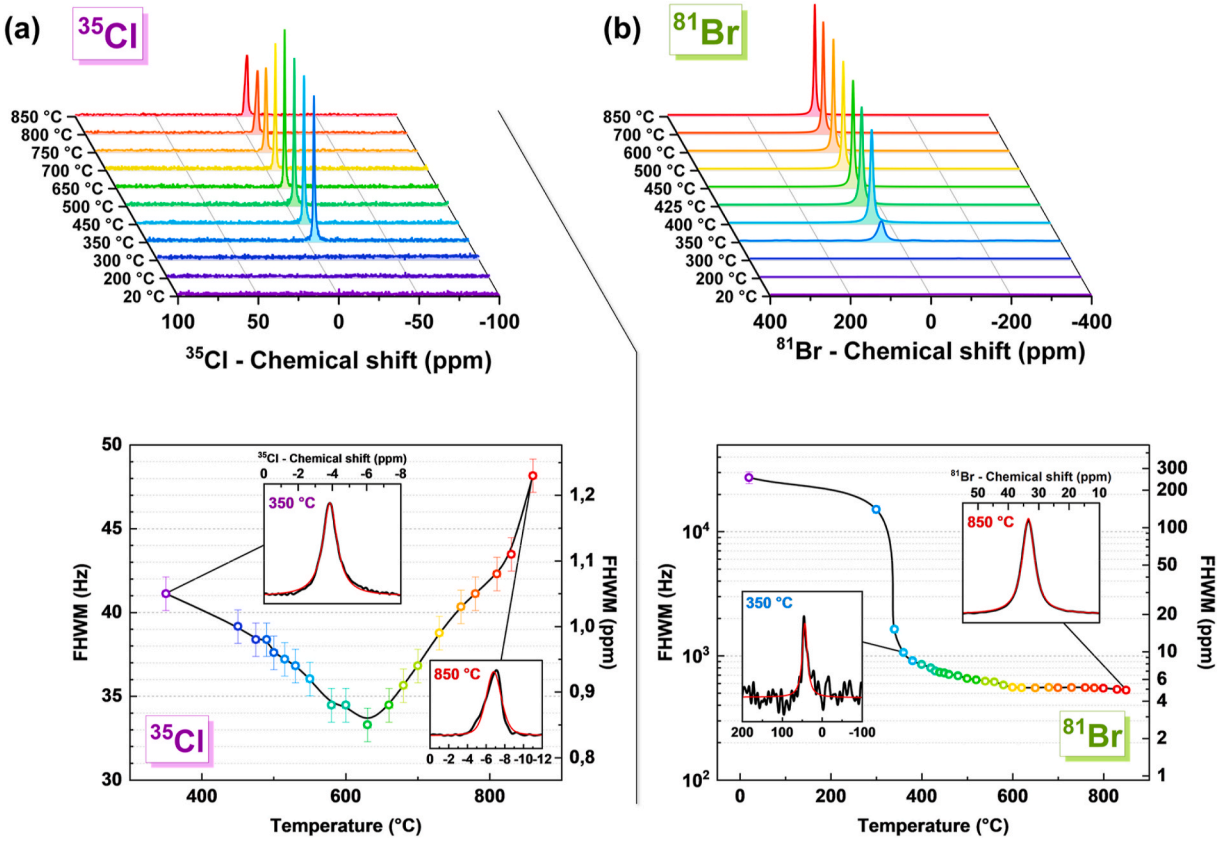

Fig. 6. (a) ^{35}Cl spectra and linewidth evolution as a function of temperature. (b) ^{81}Br spectra and linewidth evolution as a function of temperature (B_0 = 9.4 T, static HT-NMR).

3.4. Impact of binding and pellet density on lithium mobility

Binding has a significant impact on electrical conductivity and, consequently, on electrolyte performance. Fig. 8 (a) highlights this effect by comparing the electrical conductivity of the salts alone with that measured in a separator pellet (80 % TMD, Ø10 mm, 1 mm thick). Conductivity is roughly halved after binding the salts.

However, the activation energy determined from conductivity

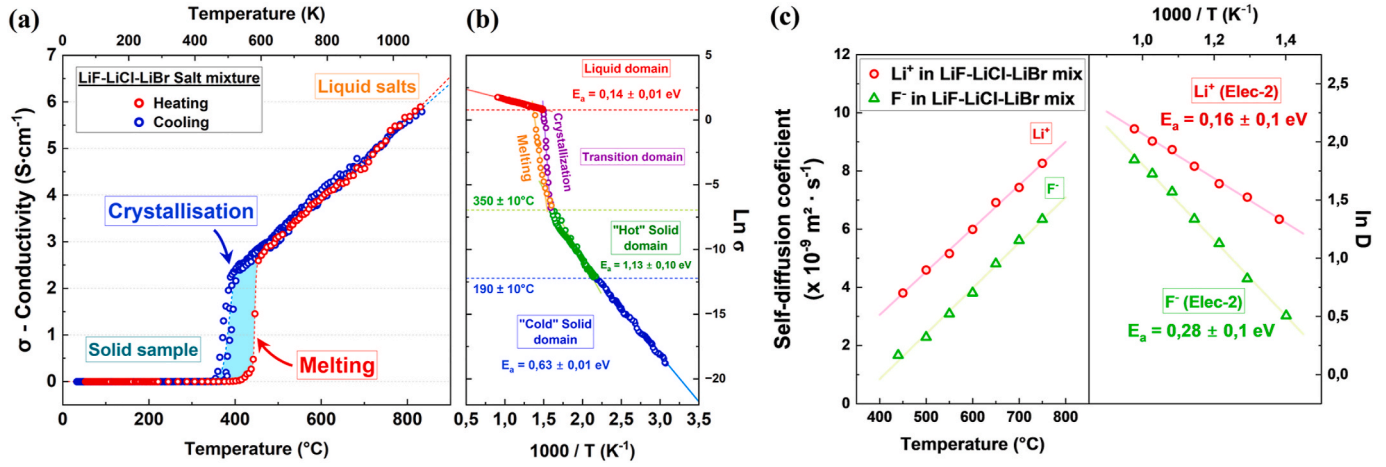

Fig. 7. (a) Heating and cooling electrical conductivity curves obtained by EIS on a bulk sample of the LiF-LiCl-LiBr eutectic mixture. (b) Arrhenius plot of electrical conductivity. (c) ^{7}Li & ^{19}F self-diffusion coefficient obtained on LiF-LiCl-LiBr molten mixture by PFG-NMR and associated Arrhenius plot.

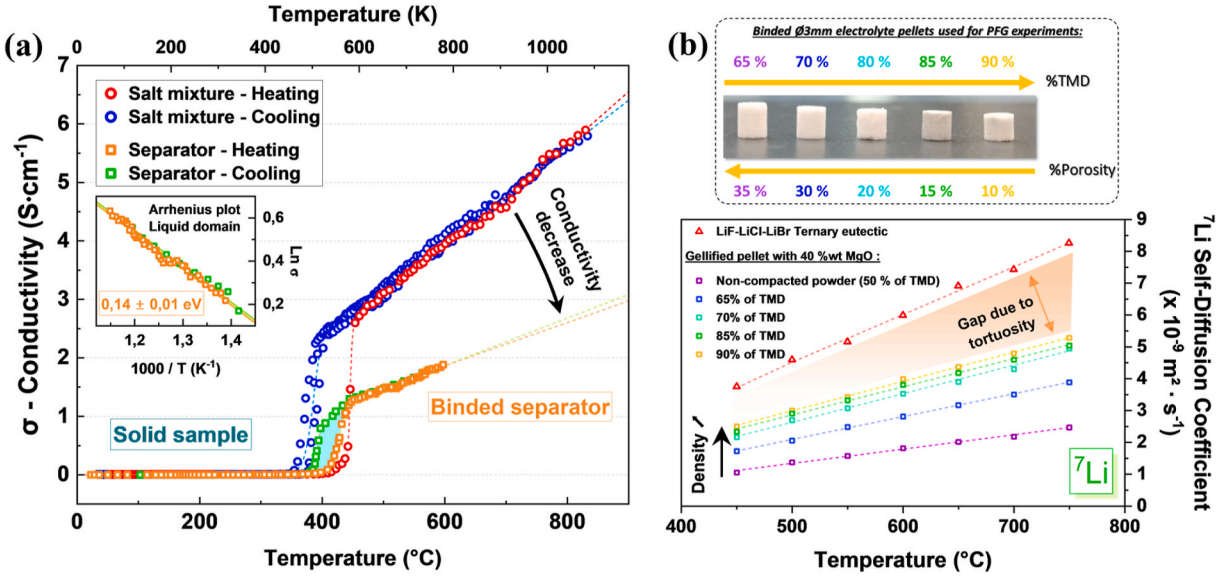

Fig. 8. (a) Temperature dependent electrical conductivity measurements on the LiF-LiCl-LiBr salt mixture and its bound form. (b) Impact of binding and separator pellet density on lithium mobility.

measurements above the melting point of the salts remains the same in both systems (Ea = 0.14 eV), with only a significant variation in the pre-exponential factor. This suggests that the reduction in conductivity caused by the binder is primarily due to the effects of the medium's tortuosity and porosity.

To confirm that this effect results from the addition of a non-conductive agent and the tortuosity it introduces, we supplemented this study with HT-PFG NMR analyses on separator pellets of varying densities. Pellet porosity was determined by comparing the density obtained from the mass and dimensions of the pellets to the material's theoretical maximum density (TMD). These results are presented in Fig. 8 (b).

Binding directly reduces the mobility of lithium cations in the molten phase of the separator. This effect becomes more pronounced in high-porosity pellets. Lithium mobility increases with the sample's density, with a particularly significant rise observed when transitioning from 65 % TMD to 80 % TMD.

However, beyond this density, the effect diminishes and seems to approach a limit. This increase in mobility is attributed to the reduced influence of porosity within the sample, which otherwise hinders the movement of ionic species.

At higher densities, the impact of the pellet's tortuosity becomes more significant. This property accounts for the differences observed between the curves corresponding to highly dense pellets and those of the molten salt mixture without binder.

4. Discussion

To begin with the behavior of the system in the solid state, the first point deals with the solid solution formed between LiCl and LiBr. This solid solution appears continuous and homogeneous from room temperature up to the melting point of the salt mixture. The substitution between the two anions is consistent with their similar ionic radii, 1.88 Å for Cl^- and 2.01 Å for Br^- [54], representing a difference of less than 7 %. Their electronegativity values are also fairly close, with 3.16 for chlorine and 2.96 for bromine [55].

In contrast, XRD and SEM-EDS analyses show that LiF does not form a solid solution with the other components; instead, it remains distinct and physically separated from the LiCl-LiBr solid solution. This behavior can be explained by the Hume-Rothery rules: although fluorine,

chlorine, and bromine share the same valence, the ionic radius of F^- (1.44 Å [54]) and its electronegativity (3.98 [55]) differ too significantly from those of Cl^- and Br^- to allow for substitution within the crystal lattice.

The electrical conductivity of the unbound LiF-LiCl-LiBr salt mixture exhibits different behaviors depending on the temperature range. In the solid state, conductivity appears complex and is directly influenced by the activation of specific ionic species mobility. The sample behaves as an electrical insulator up to 200 °C. Beyond this temperature, conductivity is primarily governed by lithium mobility in the solid state, up to 350 °C.

At this point, contributions from the mobility of chlorine and bromine ions are also detected, still within the solid phases, accompanied by a significant increase in activation energy. This rise in activation energy reflects the destabilization of the solid system. Fluorine begins to exhibit mobility at a later stage, around 420 °C, just before the mixture melts. Once the salts are fully molten, beyond 440 °C, conductivity shows a very low activation energy and follows typical Arrhenius behavior. The values of the Arrhenius parameters, determined from experimental measurements for both the pure salts and a bound pellet at 80 % TMD, are summarized in Table 3.

In the solid-state ternary system, ionic conductivity is primarily governed by the mobility of lithium ions. Lithium migrates through the material via crystal defects, whose concentration increases with temperature. As a result, ionic conductivity improves at higher temperatures due to the enhanced formation of these defects. This explains why no significant conductivity is observed below 200 °C.

Among the phases present, LiF is noticeably more stable than LiCl, LiBr, or the Li(Cl,Br) solid solution. This greater stability is attributed to the much larger electronegativity difference between lithium and fluorine, which results in stronger ionic bonding compared to the bonds formed with chlorine or bromine, and results in a higher melting temperature for LiF (848 °C) compared to LiCl (605 °C) and LiBr (552 °C). Additionally, the considerable mismatch in ionic radii between lithium and the larger halide ions (Cl^- and Br^-) favors the formation of structural defects in LiCl, LiBr, and their solid solution, but not in LiF.

Because of its higher stability, LiF is less prone to defect formation, making it less favorable for lithium ion migration. In contrast, lithium ions can more easily diffuse through the defect-rich LiCl and LiBr phases, or their solid solution.

Lithium can also move between the different lithium-containing phases and may substitute into the LiF lattice, whereas fluorine remains immobile due to its inability to substitute into other phases. As a result, fluorine forms a rigid structural framework through which lithium ions diffuse—until temperatures exceed around 420 °C, at which point even the fluorine sublattice begins to experience bond disruption, enabling further mobility.

The same approach can be applied to the self-diffusion coefficient of ionic species in molten salts. The fitting parameters for the self-diffusion coefficients of lithium and fluorine in the salt mixture, as well as lithium in bound pellets at different densities, are compiled in Table 4.

Fluorine diffusion in molten salts requires significantly more activation energy compared to lithium. Consequently, lithium serves as the primary charge carrier in this salt mixture, making its mobility a valuable indicator of the electrolyte's performance.

Analysis of lithium behavior in bound pellets shows that pellet density mainly affects the pre-exponential factor, while the activation energy remains nearly constant across the density range (50–90 % TMD).

This finding suggests that the enhanced lithium mobility in dense pellets, compared to loosely packed ones, does not result from a new diffusion mechanism, as the activation energy shows no notable variation. Instead, this increased mobility arises solely from reduced porosity, which eliminates dead volumes where ions cannot move.

Furthermore, fluorine diffusion is no longer detectable, as its relaxation becomes too rapid to allow PFG measurements, likely due to its reduced mobility in the mixture. The detection limit of PFG-NMR for measuring the self-diffusion coefficient of fluorine under these conditions is in the order of 10^{-14} m^2 s^{-1}. This suggests that binding has a much stronger impact on the mobility of fluorine compared to that of lithium. Such a result may indicate a specific interaction between the molten fluorides and the oxide matrix. Further studies are needed to better understand this potential interaction.

Increasing pellet density is key to improving the separator's electrochemical performance. However, excessive densification can result in the loss of salt retention by the binder, causing salts to leak from the pellet edges. This phenomenon, known as electrolyte leakage, becomes more pronounced at high temperatures as the salts become more fluid. Such leakage leads to a significant increase in separator resistance, ultimately impairing cell performance. In severe cases, excessive leakage may lead to collapse of the separator and allow direct contact between the positive and negative electrodes, causing a short circuit.

Observations using the PFG method on pellets exceeding 90 % TMD at temperatures above 500 °C have confirmed this behavior. The lithium signal then exhibits a highly mobile secondary component, comparable to that of the free salt, indicating that the binder is no longer fulfilling its role. This high-temperature NMR approach also provides a means to determine the optimal binder content and pellet density to maximize separator performance.

Compared to the binary LiCl-KCl system, the ternary system exhibits nearly twice the electrical conductivity, with values around 3.21 S·cm-1 versus 1.74 S·cm-1 for the binary mixture. However, the lithium self-diffusion coefficients at 500 °C are relatively similar in both systems, ranging from approximately 4 to 6 × 10-9 m2·s-1. This indicates that lithium diffuses at comparable rates in both electrolytes, yet the ternary system delivers nearly double the electrochemical performance.

If this difference in performance can be partly attributed to the higher lithium content in the ternary electrolyte (50 at% Li compared to 29 at% Li in LiCl-KCl), this discrepancy can be also explained by the more complex ionic mobility mechanisms in the LiCl-KCl binary system, where strong competitive interactions between different cations tend to hinder electrolyte performance. Overall, the ternary mixture demonstrates a more favorable behavior and appears significantly better suited for applications requiring high-current discharges. The ionic behavior in the LiCl-KCl system will be the subject of a follow-up study using the same methodology, as there is still much to explore.

Table 3
Empiric parameters for electrical conductivity of liquid LiF-LiCl-LiBr molten salt and 80 %TMD binded pellet.

Sample	σ_0 (S·cm^{-1})	E_a (ev)
Salt mixture	24.68 (±0.40)	0.138 (±0.002)
Binded pellet (80 %TMD)	12.62 (±0.05)	0.144 (±0.001)

Table 4
Empiric parameters for self-diffusion coefficient of ionic species in molten salt and binded pellets.

Salt mixture		
Ion	D_0 ($\times 10^{-9}$ m^2 s^{-1})	E_a (ev)
Li^+	53.50 (±0.05)	0.164 (±0.001)
F^-	155.90 (±0.05)	0.279 (±0.001)
Binded pellet (Li^+)		
Density	D_0 ($\times 10^{-9}$ m^2 s^{-1})	E_a (ev)
50 %TMD	17.5 (±1.06)	0.172 (±0.001)
65 %TMD	27.5 (±1.04)	0.172 (±0.001)
70 %TMD	30.9 (±1.07)	0.167 (±0.001)
85 %TMD	31.6 (±1.07)	0.159 (±0.001)
90 %TMD	32.5 (±1.11)	0.157 (±0.001)

5. Conclusion

This study investigated the transport properties of Li^+ and F^- in the molten salt mixture LiF-LiCl-LiBr, a commonly used electrolyte in thermal batteries that remains underexplored in the literature. The study combined electrical conductivity measurements using electrochemical impedance spectroscopy (with a four-electrode setup), qualitative assessment of ion mobility through HT-NMR, and quantitative determination of lithium and fluorine self-diffusion coefficients via PFG-NMR. The results confirmed that lithium serves as the primary charge carrier in this system, diffusing significantly faster than fluorine. Its mobility increases with temperature in a typical Arrhenius-like manner for ionic liquids.

We extended this innovative methodological approach to bound pellets containing MgO alongside the molten salts. The results demonstrated that the addition of the binding agent reduces ion mobility and lowers the separator's electrical conductivity. However, the activation energy for conductivity or lithium diffusion shows minimal variation between pure salts and their bound forms. This indicates that the performance reduction caused by binding stems from mechanical rather than chemical effects. Additionally, pellet density emerged as a critical parameter to optimize separator design.

CRediT authorship contribution statement

Clément Hachem: Writing – original draft, Visualization, Methodology, Investigation, Formal analysis, Data curation, Conceptualization. **Luc Faget:** Writing – review & editing, Supervision, Resources, Project administration, Funding acquisition, Conceptualization. **Emmanuel Veron:** Writing – review & editing, Methodology. **Catherine Bessada:** Writing – review & editing, Funding acquisition. **Leire Del Campo:** Writing – review & editing, Methodology. **Arthur Cachot:** Writing – review & editing, Methodology. **Lionel Cosson:** Methodology. **Vincent Sarou-Kanian:** Writing – review & editing, Methodology. **Michaël Deschamps:** Writing – review & editing, Supervision, Project administration, Conceptualization.

Declaration of competing interest

The authors declare the following financial interests/personal relationships which may be considered as potential competing interests: Clement Hachem reports financial support and equipment, drugs, or supplies were provided by ASB Aerospatial Batteries. Clement Hachem reports financial support was provided by ANRT Association Nationale de la Recherche et de la Technologie. Clement Hachem reports a relationship with ASB Aerospatial Batteries that includes: employment. If there are other authors, they declare that they have no known competing financial interests or personal relationships that could have appeared to influence the work reported in this paper.

Acknowledgement

The authors gratefully acknowledge the financial and material support of ASB Aerospatiale Batteries for this study. This material is based upon work supported by the ANRT (Association nationale de la recherche et de la technologie) with a CIFRE fellowship granted to Clément Hachem.

Appendix A. Supplementary data

Supplementary data to this article can be found online at https://doi.org/10.1016/j.jpowsour.2025.237558.

Data availability

Data will be made available on request.

References

[1] R.A. Guidotti, P. Masset, Thermally activated ("thermal") battery technology: part I: an overview, J. Power Sources 161 (2) (2006) 1443–1449.
[2] N. Schuster, A Breakthrough in Thermal Battery Performance-Expanding the Envelope to Multi-HOUR Missile/Aircraft Missions (No. 971217), 1997. SAE Technical Paper.
[3] P. Mosier-Boss, S. Szpak, Electrochemical systems with high power density: an overview, Naval Ocean Syste. Center (1989) (Technical Document 1715 - AD-A221 783) 9-16.
[4] G. Dée, T. Vanthuyne, A. Potini, I. Pardos, G. De Crombrugghe, Electromechanical thrust vector control systems for the Vega-C launcher, in: Proceedings of the 8th European Conference for Aeronautics and Space Sciences (EUCASS 2019), Madrid, Spain, 2019, July, pp. 1–4.
[5] R.A. Guidotti, F.W. Reinhardt, J. Odinek, Overview of high-temperature batteries for geothermal and oil/gas borehole power sources, J. Power Sources 136 (2) (2004) 257–262.
[6] J.R. Sweeney, I. McKirdy, R. Comrie, I. Stewart, Some advances in the application of thermal battery technology, ASB Group. Aerospace Energetic Equipment Conference, Avignon – France, November (2004). Conference paper.
[7] P. Masset, R.A. Guidotti, Thermal activated (thermal) battery technology: part II. Molten salt electrolytes, J. Power Sources 164 (1) (2007) 397–414.
[8] P. Masset, S. Schoeffert, J.Y. Poinso, J.C. Poignet, Retained molten salt electrolytes in thermal batteries, J. Power Sources 139 (1–2) (2005) 356–365.
[9] P.J. Masset, R.A. Guidotti, Thermal activated ("thermal") battery technology: part IIIa: feS2 cathode material, J. Power Sources 177 (2) (2008) 595–609.
[10] P.J. Masset, R.A. Guidotti, Thermal activated ("thermal") battery technology: part IIIb. Sulfur and oxide-based cathode materials, J. Power Sources 178 (1) (2008) 456–466.
[11] R.A. Guidotti, P.J. Masset, Thermally activated ("thermal") battery technology: part IV. Anode materials, J. Power Sources 183 (1) (2008) 388–398.
[12] J.H. Cho, C.N. Im, C.H. Choi, S.H. Ha, H.K. Yoon, Y. Choi, J. Bae, Thermal stability characteristics of high-power, large-capacity, reserve thermal batteries with pure li and li (si) anodes, Electrochim. Acta 353 (2020) 136612.
[13] Z. Tomczuk, S.K. Preto, M.F. Roche, Reactions of FeS electrodes in LiCl-KCl electrolyte, J. Electrochem. Soc. 128 (4) (1981) 760.
[14] R.A. Guidotti, F.W. Reinhardt, Electrolyte Effects in Li (Si)/FeS2 Thermal Batteries (No. SAND-94-1870C; CONF-950461-1), Sandia National Labs., Albuquerque, NM (United States), 1994.
[15] P. Singh, R.A. Guidotti, D. Reisnerc, Ac impedance measurements of molten salt thermal batteries, J. Power Sources 138 (1–2) (2004) 323–326.
[16] K. Sridharan, T. Allen, M. Anderson, M. Simpson, Thermal Properties of LiCl-KCl Molten Salt for Nuclear Waste Separation (No. DOE/NEUP-09-780), Univ. of Wisconsin, Madison, WI (United States); Idaho National Lab.(INL), Idaho Falls, ID (United States), 2012.
[17] J.P. Glatz, R. Malmbeck, P. Souček, B. Claux, R. Meier, M. Ougier, T. Murakami, Development of pyrochemical separation processes for recovery of actinides from spent nuclear fuel in molten LiCl-KCl, in: Molten Salts Chemistry, Elsevier, 2013, pp. 541–560.
[18] A. Mullabaev, O. Tkacheva, V. Shishkin, V. Kovrov, Y. Zaikov, L. Sukhanov, Y. Mochalov, Properties of the LiCl-KCl-Li2O system as operating medium for pyrochemical reprocessing of spent nuclear fuel, J. Nucl. Mater. 500 (2018) 235–241.
[19] P. Masset, Electrolytes « Sels Fondus » Pour Les Générateurs Dits « Thermiques » : Problématique Et Voies D'Optimisation, Thèse de doctorat, Grenoble INPG, 2002.
[20] H. Tsukamoto, M. Terasaki, Effect of electrolyte on discharge characteristics of positive electrode of Li-Al/LiCl-KCl/FeS2 thermal batteries, GS News Tech. Rep. 47 (1) (1988).
[21] C.E. Vallet, D.E. Heatherly, L. Heatherly, J. Braunstein, Electrolytic LiCl precipitation from LiCl-KCl melt in porous li-al anodes, J. Electrochem. Soc. 130 (12) (1983) 2370.
[22] Z. Tomczuk, B. Tani, N.C. Otto, M.F. Roche, D.R. Vissers, Phase relationships in positive electrodes of high temperature Li-Al/LiCl-KCl/FeS2 cells, J. Electrochem. Soc. 129 (5) (1982) 925.
[23] R.A. Guidotti, W. Reinhardt, Characterization of Mgo Powders for Use in Thermal Batteries (No. SAND-90-2104), Sandia National Lab.(SNL-NM), Albuquerque, NM (United States), 1996.
[24] X. Huang, J. Liu, M. Zeng, X. Yang, X. Liu, Effects of different MgO fiber structures on adhesive capacity and ionic migration of Li–Si/LiCl–KCl/FeS2 thermal batteries, Electrochim. Acta 324 (2019) 134918.
[25] V. Krishnamoorthy, D. Smith, N. Berg, S. Stuart, G.L. Di, L.M. Benedetto, K. Blecker, Development of magnesium oxide (MgO) binder for thermal batteries. 49th Power Sources Conference. June 27-29, 2023, National Harbor, MD, USA, 2023.
[26] F.M. Delnick, R.A. Guidotti, Ionic conduction in porous media, J. Electrochem. Soc. 137 (1) (1990) 11.
[27] R.A. Guidotti, F.W. Reinhardt, A.H. Andazola, Blending Study of Mgo-based Separator Materials for Thermal Batteries (No. SAND2002-1458), Sandia National Lab.(SNL-NM), Albuquerque, NM (United States); Sandia National Lab.(SNL-CA), Livermore, CA (United States), 2002.
[28] A. Revil, P.W.J. Glover, Theory of ionic-surface electrical conduction in porous media, Phys. Rev. B 55 (3) (1997) 1757.
[29] M.H. Miles, Exploration of molten hydroxide electrochemistry for thermal battery applications, J. Appl. Electrochem. 33 (2003) 1011–1016.
[30] P. Masset, S. Schoeffert, J.Y. Poinso, J.C. Poignet, LiF-LiCl-LiI vs. LiF-LiBr-KBr as molten salt electrolyte in thermal batteries, J. Electrochem. Soc. 152 (2) (2005) A405.

[31] S. Fujiwara, M. Inaba, A. Tasaka, New molten salt systems for high temperature molten salt batteries: ternary and Quaternary molten salt systems based on LiF–LiCl, LiF–LiBr, and LiCl–LiBr, J. Power Sources 196 (8) (2011) 4012–4018.
[32] X. Liu, J. Liu, X. Liu, Z. Yang, H. Yu, F. Wang, Porous magnesia fibers as an immobilizing agent for molten salt in thermal batteries, J. Electrochem. Soc. 163 (5) (2016) A617.
[33] L. Lu, J. Liu, Z. Yang, X. Liu, H. Yu, H. Li, F. Wang, Hydrofluoric acid modified porous magnesia fibers as immobilizing agent for molten electrolyte in thermal battery, Electrochemistry 85 (8) (2017) 451–455.
[34] K. Xia, H. Guo, J. Hu, L. Tang, Y. Wang, J. Long, Porous mullite fiber nonwoven separator materials containing Nano-MgO particles for the design of thermal batteries, Mater. Lett. 297 (2021) 130007.
[35] A. Yazdani, M. Sanghadasa, G.G. Botte, Integration of ceramic felt as separator/electrolyte in lithium salt thermal batteries and the prospect of rechargeability, J. Power Sources 521 (2022) 230967.
[36] H.W. Cheong, S.H. Ha, Y.S. Choi, Surface modified ceramic fiber separators for thermal batteries, J. Ceram. Process. Res. 13 (2) (2012) 308–311.
[37] S.H. Chae, S.H. Kang, H.W. Cheong, Y.S. Han, D.H. Yoon, Thermal batteries with ceramic felt separators–part 1: wetting, loading behavior and chemical stability, Ceram. Int. 43 (5) (2017) 4015–4022.
[38] Y. Nong, L. Fu, J. Zhu, W. Yang, D. Li, L. Zhou, Low resistance separator with hexagonal boron nitride (h-BN) binder for high power thermal battery, Mater. Chem. Phys. 296 (2023) 127221.
[39] A.L. Rollet, V. Sarou-Kanian, C. Bessada, Self-diffusion coefficient measurements at high temperature by PFG NMR, C. R. Chim. 13 (4) (2010) 399–404.
[40] T. Ohkubo, M. Gobet, V. Sarou-Kanian, C. Bessada, M. Nozawa, Y. Iwadate, Self-diffusion coefficient of lithium in molten xLi2O–(1 X) B2O3 system using high-temperature PFG NMR, Chem. Phys. Lett. 530 (2012) 61–63.
[41] A. Zhadan, V. Sarou-Kanian, L. Del Campo, L. Cosson, M. Malki, C. Bessada, Speciation and transport properties in molten alkali carbonates at high temperature, J. Phys. Chem. C 126 (40) (2022) 17234–17242.
[42] A.L. Rollet, V. Sarou-Kanian, C. Bessada, Measuring self-diffusion coefficients up to 1500 K: a powerful tool to investigate the dynamics and the local structure of inorganic melts, Inorg. Chem. 48 (23) (2009) 10972–10975.
[43] F. Gaillard, M. Malki, G. Iacono-Marziano, M. Pichavant, B. Scaillet, Carbonatite melts and electrical conductivity in the asthenosphere, Science 322 (5906) (2008) 1363–1365.
[44] C. Simonnet, J. Phalippou, M. Malki, A. Grandjean, Electrical conductivity measurements of oxides from molten state to glassy state, Rev. Sci. Instrum. 74 (5) (2003) 2805–2810.
[45] A. Pommier, F. Gaillard, M. Malki, M. Pichavant, Methodological re-evaluation of the electrical conductivity of silicate melts, Am. Mineral. 95 (2–3) (2010) 284–291.
[46] A. Cachot, L. del Campo, L. Cosson, S. Ory, E. Veron, M. Malki, Highlighting amorphous phase separation process on cooling borosilicate melts using impedance spectroscopy, J. Non-Cryst. Solids 641 (2024) 123155.
[47] D. Massiot, D. Trumeau, B. Touzo, I. Farnan, J.C. Rifflet, A. Douy, J.P. Coutures, Structure and dynamics of CaAl2O4 from liquid to glass: a high-temperature 27Al NMR time-resolved study, J. Phys. Chem. 99 (44) (1995) 16455–16459.
[48] L. Bonafous, B. Ollivier, Y. Auger, H. Chaudret, C. Bessada, D. Massiot, J. P. Coutures, High temperature NMR observation of Mobile phases up to 1500 C, J. Chim. Phys. Phys. Chim. Biol. 92 (1995) 1867, 1867.
[49] V. Lacassagne, C. Bessada, B. Ollivier, D. Massiot, P. Florian, J.P. Coutures, Étude de la transition solide/liquide de la cryolithe par résonance magnétique nucléaire de 27Al, 23Na et 19F, Comptes Rendus Acad. Sci. - Ser. IIB Mech. Phys., Chem., Astron. 325 (2) (1997) 91–98.
[50] K.S. Han, J.D. Bazak, Y. Chen, T.R. Graham, N.M. Washton, J.Z. Hu, K.T. Mueller, Pulsed field gradient nuclear magnetic resonance and diffusion analysis in battery research, Chem. Mater. 33 (22) (2021) 8562–8590.
[51] E.O. Stejskal, J.E. Tanner, Spin diffusion measurements: spin echoes in the presence of a time-dependent field gradient, J. Chem. Phys. 42 (1) (1965) 288–292.
[52] A.V. Tobolsky, Solid solutions of the alkali halides, J. Chem. Phys. 10 (3) (1942) 187–192.
[53] J.L. Bjorkstam, J. Listerud, M. Villa, C.I. Massara, Motional narrowing of a gaussian NMR line, J. Magn. Reson. 65 (3) (1985) 383–394.
[54] M. Rahm, R. Hoffmann, N.W. Ashcroft, Atomic and ionic radii of elements 1–96, Chem.–Eur. J. 22 (41) (2016) 14625–14632.
[55] L.R. Murphy, T.L. Meek, A.L. Allred, L.C. Allen, Evaluation and test of pauling's electronegativity scale, J. Phys. Chem. 104 (24) (2000) 5867–5871.